Superstrong Ultralong Carbon Nanotubes for Mechanical Energy Storage

Rufan Zhang, Qian Wen, Weizhong Qian, Dang Sheng Su, Qiang Zhang, and Fei Wei*

Energy storage in a proper form is essential for a good grid strategy. The systems developed so far mostly use batteries or capacitors in which energy is stored electrochemically or electrostatically. Mechanical energy storage is also one of the most important ways for energy conversion. In fact, water reservoirs on high mountains store mechanical energy using the gravitational potential on the earth, and the surplus energy can be mechanically stored in water pumped to a higher elevation using pumped storage methods. Other systems for mechanical energy storage were realized, such as flywheels storing mechanical energies by the use of a rapidly rotating mass and steel springs storing mechanical energies by their elasticity. However, such mechanical energy storage usually is operated on a macroscopic scale, and the energy density is not very high. With the fast development of nano- and micro-electromechanical systems (N/MEMS) and actuators, nanoscale mechanical energy storage is highly required.

Developing a robust nonmaterial with good mechanical performance and stable supply is the first step. Ultralong carbon nanotubes (CNTs) with the properties of 1–2 TPa modulus and 100–200 GPa strength,[1–4] the strongest material ever known, have shown promising potential for the storage of mechanical energy, either by their deformation in the composite materials,[5–7] or by their elastic deformation produced by stretching or compressing the pristine tubes or tube arrays.[8] Theoretical calculation suggested that the energy storage capacity, in the latter case, can be at least three orders higher than that of steel spring and several times that of the flywheels and lithium ion batteries.[9,10] The mechanical energy storage capacity of CNTs depends on their mechanical properties, while which directly depend on their molecular structures. Besides, CNTs that simultaneously have theoretically high strength (100–200 GPa), high tensile modulus (1–2 TPa) and high breaking strain (>15%) are not yet experimentally available on the macroscale.[2,11–20] This

is mainly due to the existence of defects in the fabricated CNTs. Even for CNTs with little defects, the highest reported breaking strain is 13.7% ± 0.3%,[21] which is still lower than the theoretical value.[22,23]

Here we experimentally demonstrate that the as-grown defect-free CNTs with length over 10 cm, have breaking strain up to 17.5%, tensile strength up to 200 GPa and Young's modulus up to 1.34 TPa. They could endure a continuously repeated mechanical strain-release test for over 1.8×10^8 times. The extraordinary mechanical performance qualifies them with high capacity for the storage of mechanical energy. The CNTs can store mechanical energy with a density as high as 1125 Wh kg^{-1} and a power density as high as 144 MW kg^{-1}, indicating the CNTs can be a promising medium for the storage of mechanical energy.

Recent breakthroughs in preparation techniques have made it possible to get centimeter-long CNTs with perfect graphitic structure.[24–26] To date, the length of individual ultralong CNTs has reached 20 cm,[26] which is far beyond the characterization scale of the normally used instruments, such as SEM, AFM, TEM, etc. Manipulation of individual ultralong CNTs is not an easy task due to their nanoscale diameters while macroscale lengths, which hampered measurement of their mechanical performance. To avoid the constraint of normally used instruments, we constructed a special device with individual ultralong CNT as a demonstration platform for mechanical energy storage. The device and auxiliary set-up were carried out as follows. First, millimeter-wide slots were inscribed on a silicon substrate (**Figure 1**a). Then, ultralong CNTs were grown on the substrate from the left edge to the right edge by CH$_4$ decomposition on Fe catalyst particles. Their lengths were as long as 10 cm after 20 min growth at 1000 °C. Based on the "kite mechanism",[27] ultralong CNTs floating in the gas flow during growth gradually sank down onto the silicon substrate to lie across the slots on it. Figure 1b shows four of these CNTs lying across a 0.75 mm wide slot on the substrate. Several suspended CNTs were thus naturally produced due to the strong interaction of the CNTs with the silicon substrate.[28] In this contribution, several triple walled CNTs (TWCNTs, as shown in Figure 1c) with outer diameters of 2.9–3.2 nm were selected for the mechanical performance test.

Deposition of gold nanoparticles has been used to make individual ultralong CNTs visible under optical microscopes,[29] but the strong surface tension of the liquid lets the suspended CNTs break easily during the nanoparticle deposition process. Thus, a solution-based decoration method is not suitable for the suspended CNTs. To make the suspended CNTs optically visible for the study of their mechanical performance and energy storage capacity on the macroscale, a simple but effective optical visualization method was developed. TiO$_2$ particles

R. F. Zhang, Dr. Q. Wen, Prof. W. Z. Qian, Dr. Q. Zhang, Prof. F. Wei
Beijing Key Laboratory of Green Chemical Reaction
Engineering and Technology
Department of Chemical Engineering
Tsinghua University
Beijing, 100084, China
Tel.: 8610-62785464
E-mail: wf-dce@tsinghua.edu.cn
Prof. D. S. Su
Catalysis and Materials Division
Shenyang National Laboratory for Materials Science
Institute of Metal Research
Chinese Academy of Sciences
Shenyang, 110016, China

COMMUNICATION
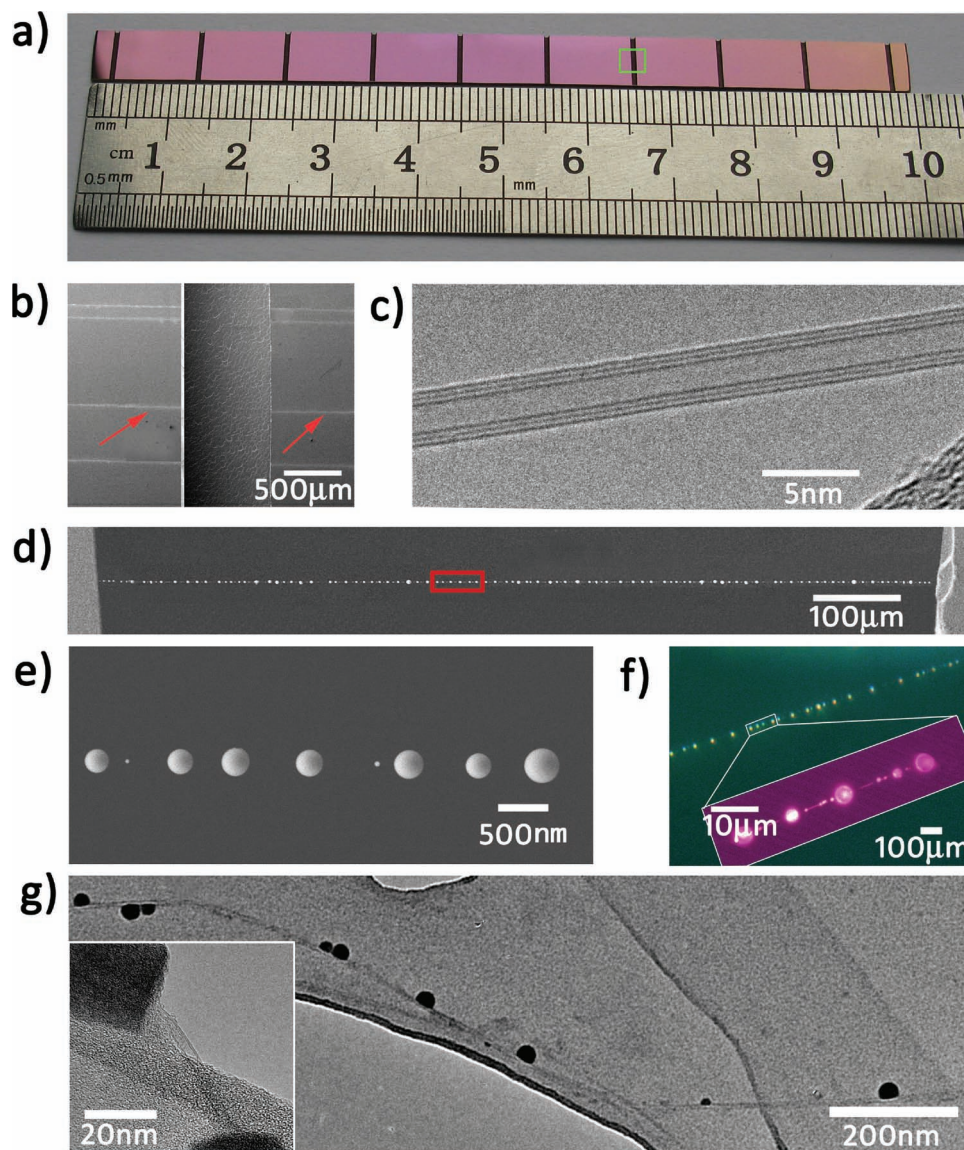
Figure 1. a) SiO$_2$ (500 nm)/silicon substrate with slots of 0.75 mm wide and 0.4 mm deep. b) SEM image of as-fabricated CNTs growing across a 0.75 mm wide slot shown by the green rectangular in panel a. c) TEM image of the triple walled CNT shown by the red arrows in panel b. d) SEM image of the suspended CNT with TiO$_2$ particles shown by the red arrows in panel b. e) part of the suspended CNT/TiO$_2$ string shown by the red rectangular in panel d. f) Optical microscope images of CNTs coated by TiO$_2$ particles. g) TEM image of CNT embedded with TiO$_2$ particles. **Inset**: High resolution TEM image of a CNT embedded with two TiO$_2$ particles. Between the particles was an uncoated CNT segment with pristine shells.

in large amounts were deposited on the suspended CNTs by the hydrolysis of TiCl$_4$ which was sprayed onto the tubes. This is shown in Figure 1d and 1f, which describes that a bead-like chain was formed across the slot on the silicon substrate. There were several hundred particles with a number density of approximately 1000 mm^{-1} along the suspended CNT. Uncoated CNT segments with pristine shells can be observed between the particles (Figure 1g). The strong brightness and reflectivity of TiO$_2$ particles upon illumination allowed us to precisely locate the position of the CNTs with an optical microscope (Figure 1f, 2c, and S1, Supporting Information). The two ends of the suspended CNTs were firmly affixed by the formation of a TiO$_2$ layer on the silicon substrate by the same method (Figure S2, Supporting Information), which prevented the slippage of their

tips during the elongating or vibrating process. A special device was designed to test the mechanical strength of the bead-like chain structure. The suspended CNT/TiO$_2$ chain can be exited to vibrate by the acoustic wave from the loudspeaker linked to a signal generator (Figure S3, Supporting Information). They can even vibrate for $>1.8 \times 10^8$ times continuously. Neither slippage of TiO$_2$ particles on CNT, or decrease in their number, nor breaking of the chain was observed. This allowed us to use it as a good mechanical testing device.

The mechanical performance measurement of the CNTs was performed by introducing a steady nitrogen flow used to blow the suspended CNTs embedded with TiO$_2$ particles (**Figure 2**a). The tips of the CNTs, which were firmly embedded in the TiO$_2$ layer on the substrate, remained fixed when the suspended part

© 2011 WILEY-VCH Verlag GmbH & Co. KGaA, Weinheim
Adv. Mater. **2011**, *23*, 3387–3391
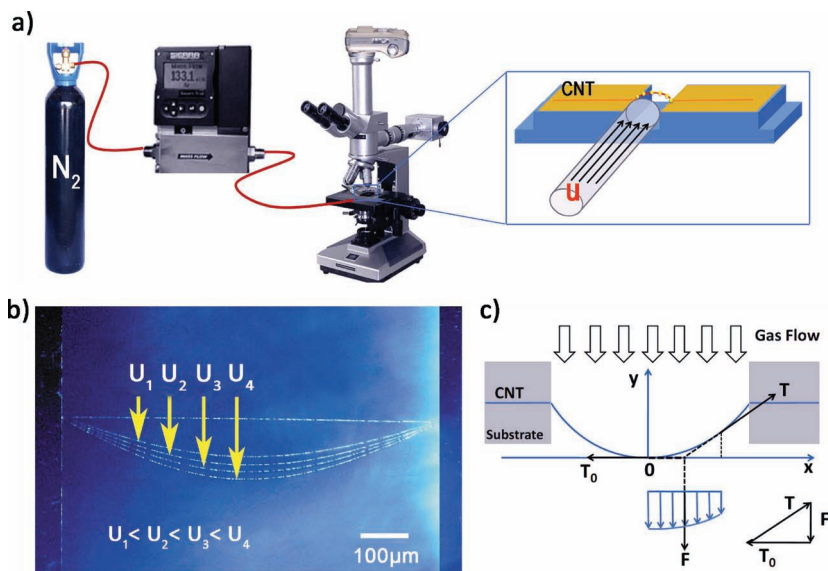
Figure 2. a) Illustration of the gas-flow-blowing system used for testing the mechanical strength of CNT/TiO$_2$ string. The suspended CNT/TiO$_2$ chain was observed using an optical microscope. The elongation of the string was recorded by a digital camera when gas flow was introduced onto the suspended tube section. U in the inset is the gas velocity. b) Elongation of the CNT/TiO$_2$ string with the increasing gas velocity. U_1, U_2, U_3 and U_4 represent different gas velocities. The two ends of the suspended CNTs remained fixed during the process. c) Force analysis illustration for a stretched CNT. T is the pull exerted along the axis of the CNT, T_0 is the pull exerted at the middle point of the suspended CNT, and F is the drag force exerted on the TiO$_2$ particles.

was stretched (Figure 2b). The elongation of the suspended CNTs was recorded by a digital camera. The three CNTs in **Figure 3**b broke when their strain reached 15.34%, 17.03%, and 17.58%, respectively. The value of 17.58% is the highest strain record for CNTs, which is higher than that reported in the literatures,[1–3,15,21,30] and is close to the upper theoretical limit for ideal CNTs.[22,23] Figure 3a is a typical Raman spectrum of the CNTs. There was a very strong G-band response centered at 1582 cm^{-1}. No D-band which was usually centered at 1310–1350 cm^{-1} was observed. The intensity of the D-band is conventionally used to detect the defect degree of CNTs.[31,32] Those characterization results indicated the perfect structure of the as-grown CNTs.

When the gas flowed through the slots on the silicon substrate, over 99% of the drag force was exerted on the TiO$_2$ particles because of their far larger cross-section compared with that of a single pristine CNT (about 3.0 nm in diameter, see Supporting Information, Text S1). The movement of the TiO$_2$ particles under the force elongated the host CNT as a tightened bowstring (Figure 2c). The stress (σ) exerted on the CNT can be determined using the force equation,

$$\sigma = \frac{T}{\pi d b} \tag{1}$$

where d is the outer diameter of the CNT (since only the outer shell of a multi-walled CNT contributes to its strength under axial tensile deformation),[3,15,22,30] b is the thickness of one single CNT shell (0.34 nm), and T is the pull exerted along the axis of the CNT (Figure 2d), which is originated from the drag

force of TiO$_2$ particles. At the end of the suspended CNT, T can be expressed as

$$T = \sqrt{T_0^2 + F_0^2} \tag{2}$$

where T_0 is the pull exerted at the middle point of the suspended CNT, and F_0 is the drag force sum exerted on all the TiO$_2$ particles (see Text S1). The Young's modulus of the tested CNTs was obtained by fitting the linear portion of their stress-strain curves (Figure 3b). The modulus values range from 1.16 to 1.51 TPa for three tested CNTs, with an average value of 1.34 TPa and an average tensile strength of 200 GPa (see Table S2). In addition, Figure 3b shows that an initial stress (10~14 GPa) exists, which was obtained from the linear fitting of the stress-strain curves. The pull of gas flow exerted on a CNT/TiO$_2$ string (T in Figure 2d) was about 10^{-7}~10^{-6} N, while the total gravity of TiO$_2$ particles on the suspended CNT was just ca. 10^{-13} N, which was negligible compared with the pull of the flow (see Text S1). According to the "kite mechanism",[27] the ultralong CNTs grew with the catalyst particles floating in the gas flow, which exerted a drag force on the growing CNTs. When the stretched floating CNTs sank down onto the silicon substrate after growth, a residual tension was retained due to the strong van der Waals force between the CNTs and silicon substrate.[28] This is the first experimental observation of simultaneously high strain (>15%), high tensile strength (~200 GPa), and high Young's modulus (~1.34 TPa) on a perfect ultralong CNT, which was higher than the reported values of Young's modulus and tensile strength of a CNT with 2-3 shells were 1.105 TPa and 97 GPa, respectively,[3] and for multi-walled CNTs with 12-19 shells, the values were between 0.95–1.049 TPa and 28–110 GPa, respectively.[3,15,30]

The high stiffness and ability of the CNTs to keep high strain render their extraordinary performance on mechanical energy storage. The gravimetric energy density is

$$u_m = \frac{1}{\rho} \frac{A}{A_T} \int_0^\varepsilon \sigma \, d\varepsilon \tag{3}$$

where $A = \pi(r_0^2 - r_1^2)$ is the cross-sectional area of the outer shell, $A_T = \pi r_0^2$ is the total enclosed area, σ is the applied stress, ε is the strain, and ρ is the density of the CNTs.[9] The highest energy densities were 1125, 1085, and 970 Wh kg^{-1} for the three CNTs in Figure 3b, respectively. The theoretical value was 1163 Wh Kg^{-1} at 17% strain (see Text S2).[33] It is shown in **Figure 4** that the CNT string system is advantageous over all existing energy storage systems, including all kinds of batteries, super-capacitors, and flywheels, both in energy density and power density.[34–36] Its energy density was nearly 3 times that of Carbon T1000 flywheels (350 Wh Kg^{-1}),[22] 5–8 times that of Li ion batteries (120–180 Wh Kg^{-1}),[37] and 25 000 times that of steel springs (0.039 Wh Kg^{-1}).[9,38]

a)

b)

c)
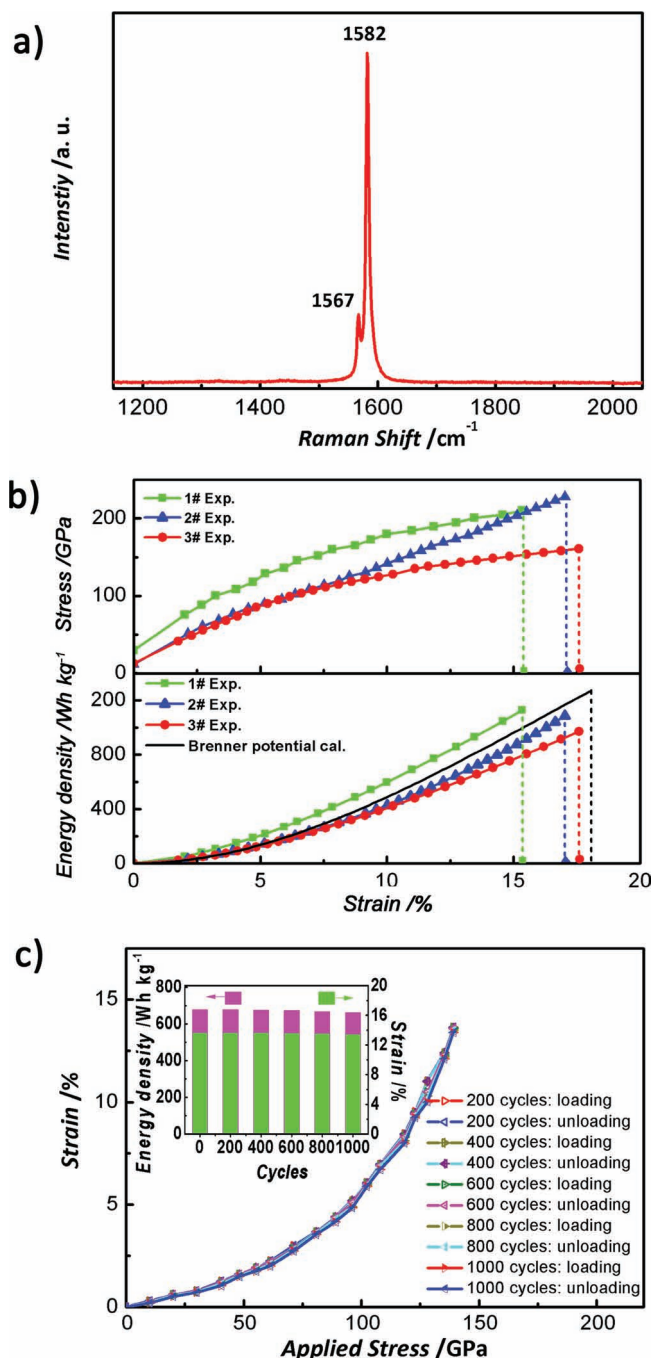
Figure 3. a) A typical Raman spectrum from the as-grown CNTs. b) Stress–strain curves and energy density–strain curves for 3 CNTs with high strain. The black line represents the energy density based on the 2nd Brenner potential method (ref. 32). c) Strain-stress behavior of a CNT after 200, 400, 600, 800, and 1000 strain-relaxation cycles. **Inset**: Energy density and strain property.

Moreover, the CNTs exhibited excellent strain-relaxation reversibility and high fatigue resistance capability. The strain-stress curves after 200, 400, 600, 800, and 1000 strain-relaxation cycles with strains of 13-16% were nearly unchanged (Figure 3c). In another test, shown in Figure S3 of the Supporting Information, the CNT/TiO$_2$ string, excited by an acoustic wave at a fixed
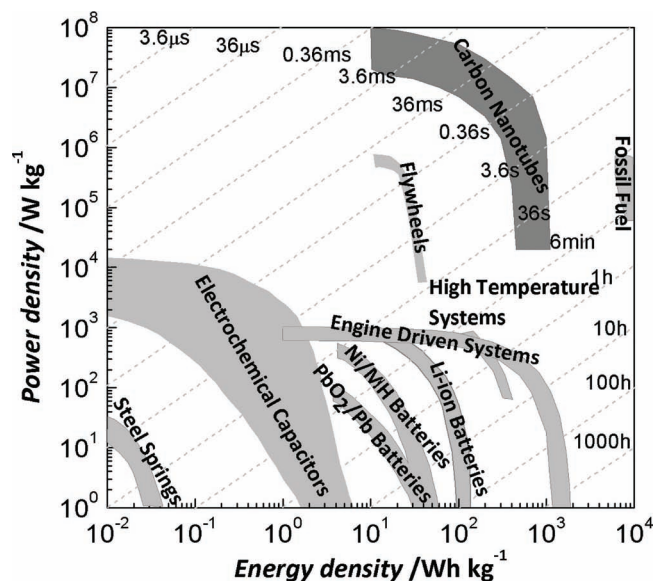
Figure 4. Ragone plot for different energy storage materials.

frequency, could vibrate continuously for 1.8×10^8 times with a strain of 0.08%, and maintained unbroken. In comparison, Li ion batteries and super-capacitors often suffer from unavoidable energy loss in charge-discharge cycles. The energy density in the vibration test case was 10 Wh Kg^{-1} and the power density was as high as 144 MW kg^{-1}, obtained from the energy density divided by the discharging time of 0.00025 s (the vibration frequency was 1000 Hz). This capacity is sufficient for the energy supply of small electronic devices including cell phones, micro-scaled sensors, watches, etc. In addition, the working mode of the individual CNTs, which were sensitive to ambient tiny vibrations, is promising for the fabrication of self-powered N/MEMS, flexible devices, sensors, actuators, and antennas.[39] In addition, the CNTs offer a cleaner and safer energy storage manner compared to batteries and super-capacitors. The further scale-up of the CNT system can have astonishing applications due to their ultrahigh strength.

In summary, we have fabricated superstrong ultralong CNTs with perfect structures and measured the mechanical properties of them. The CNTs simultaneously exhibited high strength, high Young's modulus, and large breaking strain. The high energy density and power density of CNTs made them promising materials for the storage of mechanical energy. This work also provides a structural model towards the mechanical energy storage that might be used in areas such as N/MEMS, flexible device, sensors, actuator, and antenna.

Experimental Section

Substrate preparation: Single crystal silicon slices (10 cm long, 0.5–1 cm wide, and 0.5 mm thick) were used as substrates. First, several slots (0.5-1 mm wide, 0.3-0.5 mm deep) were inscribed on the substrates using a laser etching technique. The substrates were then cleaned by acetone, ethanol, and deionized water in sequence, each for 3.0 min, in an ultrasonic bath. After that, the silicon substrates were oxidized by dry O$_2$, and then wet O$_2$, then dry O$_2$ at 1000 °C for 5, 50, and 5 min in sequence at a flow of 500 sccm. The SiO$_2$ layer was about 500 nm thick.

CNT fabrication: A solution containing catalyst precursor FeCl$_3$ in ethanol (0.03 mol L^{-1}) was daubed onto the upstream end of the silicon substrate. After reduction in H$_2$ and argon (H$_2$: Ar = 2:1 in volume with a total flow of 200 sccm) at 900 °C for 25 min, the iron precursor became iron nanoparticles that were the catalysts for the subsequent chemical vapor deposition for CNT growth at 1000 °C. CH$_4$ and H$_2$ (CH$_4$: H$_2$ = 1:2 in volume with a total flow of 75 sccm) were used as carbon source, together with 0.43% H$_2$O for accelerating CNTs growth. The growth time for the CNTs was usually 10–20 min, which depended on the length of CNTs desired.

TiO$_2$ particles deposition: A TiCl$_4$ mist was sprayed onto the suspended CNTs first. Due to the rapid hydrolysis of TiCl$_4$ in air, it soon became TiO$_2$ particles with an average diameter of 0.6 μm. There was a strong interaction between the TiO$_2$ particles and the shells of the CNTs, which made the TiO$_2$ particles very stable on the CNTs.

Characterization: The CNTs were characterized by scanning electron microscopy (SEM, JSM 7401F, 1.0 kV), high-resolution transmission electron microscopy (TEM, JEM-2010, 120.0 kV), and Raman instrument (Horiba JY, 632.8 nm). The suspended CNTs embedded with TiO$_2$ particles and their mechanical behaviour were recorded by an optical microscopy (Shanghai Optical Instrument Co. Ltd).

Supporting Information

Supporting Information is available from the Wiley Online Library or from the author.

Acknowledgements

[1] M. M. J. Treacy, T. W. J. Ebbesen, M. Gibson, *Nature* **1996**, *381*, 678.

[2] D. A. Walters, M. L. Ericson, J. M. Casavant, J. Liu, T. D. Colbert, A. K. Smith, E. R. Smalley, *Appl. Phys. Lett.* **1999**, *74*, 3803.

[3] B. Peng, M. Locascio, P. Zapol, S. Li, S. L. Mielke, G. C. Schatz, H. D. Espinosa, *Nat. Nanotechnol.* **2008**, *3*, 626.

[4] S. Iijima, T. Tichihashi, *Nature* **1993**, *363*, 603.

[5] B. C. Edwards, *Acta Astronautica* **2000**, *47*, 735.

[6] A. B. Dalton, S. Collins, E. Munoz, J. M. Razal, V. H. Ebron, J. P. Ferraris, J. N. Coleman, B. G. Kim, R. H. Baughman, *Nature* **2003**, *423*, 703.

[7] K. Koziol, J. Vilatela, A. Mosiala, M. Motta, P. Cunniff, S. Michael, A. Windle, *Science* **2007**, *318*, 1892.

[8] A. Y. Cao, P.L. Dickrell, W. G. Sawyer, M. N. Ghasemi-Nejhad, P. M. Ajayan, *Science* **2005**, *310*, 1307.

[9] F. A. Hill, T. F. Havel, C. Livermore, *Nanotechnology* **2009**, *20*, 255704.

[10] a) B. Bolund, H. Bernhoff, M. Leijon, *Renew. Sust. Energ. Rev.* **2007**, *11*, 235; b) E. Deiss, A. Wokaun, J. L. Barras, C. Daul, P. Dufek, *J. Electrochem. Soc.* **1997**, *144*, 3877.

[11] Z. W. Pan, S. S. Xie, L. Lu, B. H. Chang, L. F. Sun, W. Y. Zhou, G. Wang, D. L. Zhang, *Appl. Phys. Lett.* **1999**, *74*, 3152.

[12] J. P. Salvetat, G. A. D. Briggs, J. M. Bonard, R. R. Bacsa, A. J. Kulik, T. Stockli, N. A. Burnham, L. Forro, *Phys. Rev. Lett.* **1999**, *82*, 944.

[13] F. Li, H. M. Cheng, S. Bai, G. Su, M. S. Dresselhaus, *Appl. Phys. Lett.* **2000**, *77*, 3161.

[14] M. F. Yu, B. S. Files, S. Arepalli, R. S. Ruoff, *Phys. Rev. Lett.* **2000**, *84*, 5552.

[15] M. F. Yu, O. Lourie, M. J. Dyer, K. Moloni, T. F. Kelly, R. S. Ruoff, *Science* **2000**, *287*, 637.

[16] B. G. Demczyk, Y. M. Wang, J. Cumings, M. Hetman, W. Han, A. Zettl, R. O. Ritchie, *Mater. Sci. Eng. A* **2002**, *334*, 173.

[17] S. B. Cronin, A. K. Swan, M. S. Unlu, B. B. Goldberg, M. S. Dresselhaus, M. Tinkham, *Phys. Rev. Lett.* **2004**, *93*, 4.

[18] N. Olofsson, J. Ek-Weis, A. Eriksson, T. Idda, E. E. B. Campbell, *Nanotechnology* **2009**, *20*, 385710.

[19] R. Smajda, J. C. Andresen, M. Duchamp, R. Meunier, S. Casimirius, K. Hernadi, L. Forro, A. Magrez, *Phys. Status Solid. B* **2009**, *246*, 2457.

[20] X. L. Wei, Q. Chen, L. M. Peng, R. L. Cui, Y. Li, *J. Phys. Chem. C* **2009**, *113*, 17002.

[21] C. C. Chang, I. K. Hsu, M. Aykol, W. H. Hung, C. C. Chen, S. B. Cronin, *ACS Nano* **2010**, *4*, 5095.

[22] T. Dumitrica, M. Hua, B. I. Yakobson, *Proc. Natl. Acad. Sci. USA* **2006**, *103*, 6105.

[23] C.Y. Wei, K. Cho, D. Srivastava, *Phys. Rev. B* **2003**, *67*, 115407.

[24] L. X. Zheng, M. J. O'Connell, S. K. Doorn, X. Z. Liao, Y. H. Zhao, E. A. Akhadov, M. A. Hoffbauer, B. J. Rpoop, Q. X. Jia, R. C. Dye, D. E. Peterson, S. M. Huang, J. Liu, Y. T. Zhu, *Nat. Mater.* **2004**, *3*, 673.

[25] Q. Wen, W. Z. Qian, J. Q. Nie, A. Y. Cao, G. Q. Ning, Y. Wang, L. Hu, Q. Zhang, J. Q. Huang, F. Wei, *Adv. Mater.* **2010**, *22*, 1867.

[26] Q. Wen, R. F. Zhang, W. Z. Qian, Y. R. Wang, P. H. Tan, J. Q. Nie, F. Wei, *Chem. Mater.* **2010**, *22*, 1294.

[27] S. M. Huang, M. Woodson, R. Smalley, J. Liu, *Nano Lett.* **2004**, *4*, 1025.

[28] H. Son, G. G. Samsonidze, J. Kong, Y. Y. Zhang, X. J. Duan, J. Zhang, Z. F. Liu, M. S. Dresselhaus, *Appl. Phys. Lett.* **2007**, *90*, 253113.

[29] H. B. Chu, R. L. Cui, J. Y. Wang, J. Yang, Y. Li, *Carbon* **2011**, *49*, 1182–1188.

[30] W. Ding, L. Calabri, K. M. Kohlhaas, X. Chen, D. A. Dikin, R. S. Ruoff, *Exp. Mech.* **2007**, *47*, 25.

[31] M. S. Dresselhaus, G. Dresselhaus, A. Jorio, A. G. Souza Filho, R. Saito, *Carbon* **2002**, *40*, 2043.

[32] M. S. Dresselhaus, A. Jorio, M. Hofmann, G. Dresselhaus, R. Saito, *Nano Lett.* **2010**, *10*, 751.

[33] T. Xiao, K. Liao, *Phys. Rev. B* **2002**, *66*, 153407.

[34] P. Simon, Y. Gogotsi, *Nat. Mater.* **2008**, *7*, 845.

[35] H. Ibrahim, A. Ilinca, J. Perron, *Renew. Sust. Energ. Rev.* **2008**, *12*, 1221.

[36] P. V. Bossche, F. Vergels, J. V. Mierlo, J. Matheys, W. V. Autenboer, *J. Power. Sources* **2006**, *162*, 913.

[37] J. M. Tarascon, M. Armand, *Nature* **2001**, *414*, 359.

[38] *Fundamentals of Microfabrication* (Ed: M. Madou), CRC Press, Boca Raton, FL **2002**.

[39] Z. L. Wang, *Adv. Funct. Mater.* **2008**, *18*, 3553.